Thrust Measurements of a Helicon Plasma Source

Logan T. Williams [1] and Mitchell L. R. Walker[2]
High-Power Electric Propulsion Laboratory, Georgia Institute of Technology, Atlanta, Georgia, 30332

There is interest in using a helicon plasma source in propulsive applications as both an ion source and as a thruster. Developing a helicon thruster requires a performance baseline as a basis for future optimization and expansion. The thrust of a helicon is measured using an null-type inverted pendulum thrust stand at a pressure of 2x10^{-5} Torr through the operating range of 215-840 W RF power, 11.9 and 13.56 MHz RF frequency, 150-450 G magnetic field strength, and 1.5-4.5 mg/s propellant flow rate for argon. Maximum thrust is found to be 6.27 mN at 142 s of specific impulse, and maximum specific impulse at 377 s at 5.55 mN. Thrust is primarily increased by increasing RF power, with smaller gains from magnetic field strength and mass flow rate. Maximum efficiency is 1.37% and is limited by a combination of low mass utilization and high beam divergence.

Nomenclature

A	=	area of the exit plane
e	=	charge of an electron
g	=	acceleration due to gravity
I_c	=	collected ion current
I_{sp}	=	specific impulse
k	=	Boltzmann's constant
m_i	=	ion mass
$\dot{m}$	=	mass flow rate
$\dot{m}_i$	=	exiting ion mass flow rate
n_e	=	electron number density
p_b	=	base pressure
p_g	=	ion gauge pressure
P_{in}	=	total input power to the device
p_o	=	operating pressure
P_{RF}	=	RF power input into the device
T	=	thrust
T_e	=	electron temperature
v_i	=	ion exit velocity
$\bar{v}_i$	=	average ion exit velocity
V_{irg}	=	ion repulsion grid voltage
V_j	=	jth voltage of the IEDF
V_p	=	plasma potential
x_j	=	probability of the jth voltage in the IEDF
γ	=	beam divergence factor
χ	=	gas correction factor
η_a	=	anode efficiency
η_m	=	mass utilization efficiency
η_T	=	total efficiency

---
[1] Graduate Research Assistant, Aerospace Engineering, lwilliams@gatech.edu, AIAA Student Member.
[2] Associate Professor, Aerospace Engineering, mitchell.walker@ae.gatech.edu, AIAA Senior Member.

I. Introduction

HELICONS have been studied as high efficiency, high density plasma sources since the 1960s.[1-3] A helicon plasma source is a device that ionizes a gas by launching a helicon wave through the gas along an axial magnetic field. A helicon wave is a bounded right-hand circularly polarized electromagnetic wave with a frequency low enough that electron gyration can be neglected.[1] Helicon sources have been observed to create plasmas an order of magnitude denser than the input power would suggest.[4] The high efficiency of the helicon source was previously attributed to Landau damping[1] but later work has considered Trivelpiece-Gould (TG) wave coupling as the primary mechanism.[5,6]

While there are several uses for helicon plasmas in terrestrial applications, such plasma processing,[7] there has also been studies considering helicon sources in space propulsion. While some research considers using the helicon source as an ion generator,[8-11] other work examines the possibility of the helicon source itself as a thruster.[12,13] There is limited data on experimentally measured performance of the helicon source as a thruster. Much of the research thus far has focused on plume measurements. Several published works[14,15] use a retarding potential analyzer (RPA) to characterize the ion energy distribution, which was found to have two primary peaks: one at the plasma potential, and one at a higher potential. This higher potential is thought to be due to the acceleration of ions by a current-free double layer. Additional work examining the potential down the axis of a helicon found that a higher magnetic field increased the magnitude of the potential drop experienced by the ions.[16] Later work used the RPA to measure the ion beam current density across a plane perpendicular to the axis of the helicon.[17] Efforts to determine the thrust of the helicon include testing with a momentum flux target,[18] as well as direct thrust measurements of a helicon, which observed thrust in the range of 0-3[19] and 1-2.8[20] mN at powers up to 700 and 650 W, respectively. This work measures the thrust of a helicon plasma source using a null-type inverted pendulum thrust stand over a range of RF powers between 215 and 800 W, axial magnetic field strengths between 150 and 450 G, frequencies of 11.9 MHz and 13.56 MHz, and mass flow rates between 1.5 mg/s and 4.5 mg/s of argon.

II. Experimental Apparatus

A. Vacuum Facilities

All experiments are conducted in Vacuum Test Facility 1 (VTF-1). VTF-1 is a stainless steel vacuum chamber 4 m in diameter with a length of 7 m. Two 3800 CFM blowers and two 495 CFM rotary-vane pumps evacuate the chamber to a moderate vacuum (about 30 mTorr). High vacuum is normally reached by using six 48" diffusion pumps with a combined pumping speed of 600,000 L/s on air. The chamber pressure is measured with a BA-571 ion gauge connected to a Varian SenTorr controller with an accuracy of 20%.[21] An MKS type 247 four-channel readout in conjunction with an MKS 1179 mass flow controller regulates the gas flow into the helicon with an accuracy of 1%.[22] The base pressure of VTF-1 for these experiments is 1.5×10^{-5} Torr. Figure 1 shows a schematic of the VTF.
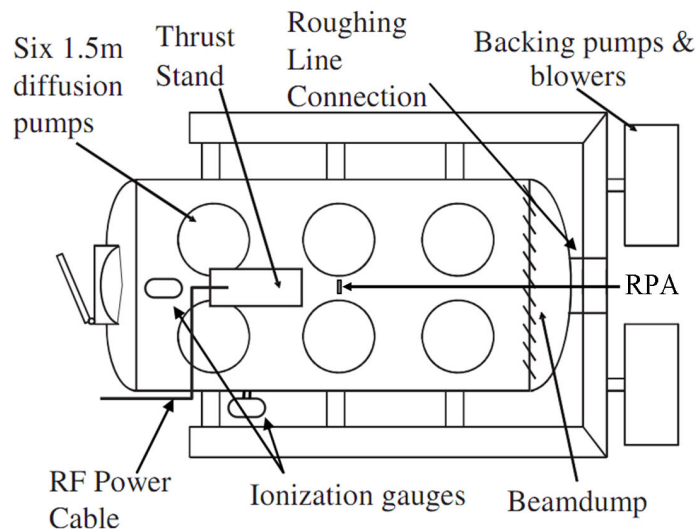

Figure 1. VTF schematic.

Operating pressure, p_o, is derived by a correction of the pressure measured by the ion gauge, given by

$$p_o = \frac{p_g - p_b}{\chi} + p_b \tag{1}$$

where p_g is the pressure given by the ion gauge, p_b is the base pressure, and χ is the gas correction factor, which is 1.29 for argon.

B. Helicon Plasma Source

Figure 2 shows the geometry of the helicon plasma source and a schematic of the RF system. The helicon consists of a Pyrex discharge chamber 27.3 cm long and 14.0 cm in diameter. The axial magnetic field is provided by two 725 turn solenoids 7.6 cm wide with a 19.7 cm inner diameter. The solenoids are placed 10.2 cm apart. Figure 3 shows the on-axis magnetic field strength for the four solenoid currents used. The magnetic field strengths are referred to by the strength at the center of the antenna; thus while the device is tested at solenoid currents of 3.76, 6.26, 8.75, and 11.25 A, they are referred to as 150, 250, 350 and 450 G, respectively. The RF signal is provided by a Yaesu FT-540 HF transceiver and amplified by an ACOM 2000A linear amplifier. A LP-100 RF wattmeter monitors the RF power transmitted, and the signal is matched by an L-type antenna tuner. RF power is transmitted through an unbalanced coaxial cable of fixed length set by RF frequency to minimize RF noise.[27] The signal is then transmitted into the plasma using a double saddle antenna centered between the solenoids. The power loss through the cable is measured beforehand with an Agilent N9912a network analyzer and used to correct the nominal power given by the wattmeter. For 11.9 MHz and 13.56 MHz the cable loss is 15.7% and 28.8%, respectively.
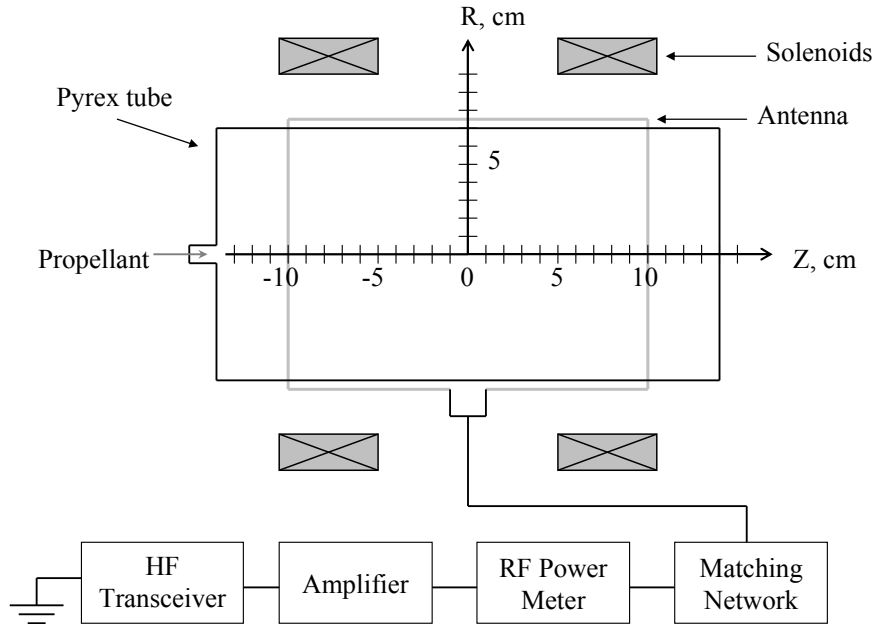

Figure 2. Helicon configuration and RF schematic.
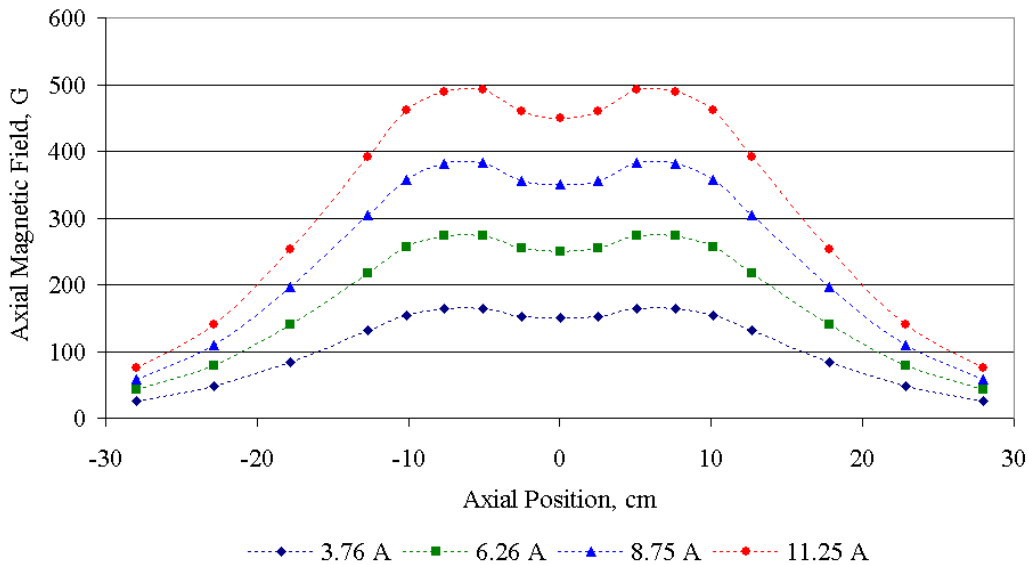
Figure 3. Centerline axial magnetic field strength at four solenoid currents.

Due to the nature of the helicon, there are two issues that must be addressed during setup to ensure accurate thrust measurement. The first is thermal drift of the thrust stand due to thermal expansion of the RF cable pushing on the antenna and producing an offset to the measurements. To prevent this, the antenna is bolted to a three axis bracing mount that fixes the antenna in place such that it does not contact either the discharge chamber or the solenoids. This allows the device to move smoothly along the axis of the thrust stand and prevents any thermal drift. Additionally, the RF cable makes a roughly 270º spiral to the antenna, allowing the cable to thermally expand along the arc, rather than expand into the antenna.

The second issue with measuring the thrust of a helicon on a thrust stand is eliminating any RF interference in the data. This appeared as a DC offset to the measured thrust stand null coil current required to maintain the thrust stand position whenever the helicon was turned on. This occurred even when the helicon was removed from the thrust stand and placed on the floor of the chamber a meter away. This was ultimately a ground loop and shielding issue with the thrust stand electronics; the solution has two parts. Inside the chamber, all signal lines are isolated from chamber ground while the cable shielding is grounded to prevent RF pickup. Outside the chamber the signal lines are still isolated from chamber ground, but the cable shielding is tied to the thrust stand electronics common ground. Each electronic component of the thrust stand is placed in a grounded enclosure tied to the common ground, which is ultimately tied to the ground of a single wall outlet. This removed all RF offset during helicon operation.

C. Diagnostics
Thrust Stand

The thrust of the helicon is measured using a null-type inverted pendulum thrust stand.[23] The thrust stand consists of two parallel plates connected by a series of four flexures that support the upper plate and allow deflection as a force is applied. A Linear Variable Differential Transformer (LVDT) measures the position of the upper plate, while two electromagnetic actuators control the motion. One actuator, the damper coil, compensates for vibrations, and the second, the null coil, holds the upper plate stationary. The thrust stand operates by using two proportional-integral-derivative (PID) control circuits that use the LVDT signal as input, and the current through one of the actuators as the output. The resulting current through the null coil is directly correlated to the solenoid current. The actual value of the thrust is determined by comparing the data to the application of a series of known calibration weights. A water-cooled copper shroud surrounds the thrust stand components to maintain thermal equilibrium. The error in the thrust stand is no greater than ±2.3 mN.

The thrust stand chiller is first run at 17 ºC overnight to bring the system to thermal equilibrium. VTF-1 is pumped down to a base pressure of 1.5×10^{-5} Torr. The thrust stand is turned on and given an hour to settle at a zero point. The driving current in the null coil of the thrust stand is digitally recorded using a LabView VI interfacing with a Keithley 2410 SourceMeter. The thrust stand is then calibrated by lowering incrementally a series of weights

American Institute of Aeronautics and Astronautics

that pull on the thrust stand and recording the thrust stand response. After calibration the mass flow controller is opened and the thrust stand given a minute to settle to record the cold gas thrust. RF waves are then broadcast into the device at 300 W to create the plasma. The two solenoids are then powered to provide the set magnetic field. The matching network is tuned to match to the plasma and the RF power is set. The thrust stand is given two minutes to settle and then the RF is turned off, with another two minutes of settling time. The difference in the thrust stand response between the plasma on and plasma off is the helicon plasma thrust contribution. The total thrust is the combination of the cold gas thrust and the helicon plasma thrust. The solenoids are then shut off and the plasma is restarted, repeating the process for each power level (eight total) for a given frequency and mass flow rate. Afterwards recording is stopped, saved, and restarted for the next frequency and mass flow. Thus, calibration occurs for every eight data points, which corresponds to on average once every eighty minutes.

Retarding Potential Analyzer
    The ion energy distribution of the thruster plume is measured with a retarding potential analyzer.[24-26] The RPA consists of four grids and a collector coaxially aligned within and isolated from a stainless steel cylinder. In order from aperture towards the collector they are the floating, electron repulsion, ion repulsion, and electron suppression grids. The floating grid has no active potential applied and becomes charged to the floating potential. This serves to reduce perturbations in the plasma caused by the presence of the other biased grids. The electron repulsion grid is negatively biased to repel plasma electrons and prevents them from reaching the collector and reducing the effective collection current. The ion repulsion grid is positively biased to retard ions and controls what ion energies are capable of reaching the collector. The electron suppression grid has a negative potential relative to the plasma to repel secondary electrons emitted due to ion collisions with the collector. Since the ion repulsion grid controls the ion current collection, the probe acts as a high pass filter, allowing only ions with energy higher than the ion repulsion grid to pass through to the collector. By sweeping the potential of the ion repulsion grid, V_{irg}, a plot of the collected ion current, I_c, as a function of the applied potential can be created. The negative derivative of this plot is proportional to the ion energy distribution. Figure 4 shows a picture of the RPA used.
    The procedure for testing with the RPA is much the same as with testing on the thrust stand. The RPA is mounted 45.08 cm downstream of the exit plane of the discharge chamber along the centerline of the device. At this distance the RPA is removed far enough from the plasma to prevent disturbances yet close enough to maintain a sufficient signal-to-noise ratio. The helicon is turned on using the same procedure above and set to a given power, frequency, and magnetic field. The RPA then scans a range of ion repulsion grid voltages from 0 to 100 V in 0.5 V increments six times. The six scans are then averaged to generate an overall I-V trace. A locally weighted scatterplot smoothing (LOESS) algorithm is used to smooth the data. The negative derivative of the ion collection current with respect to ion repulsion grid voltage is directly proportional to the ion energy distribution.
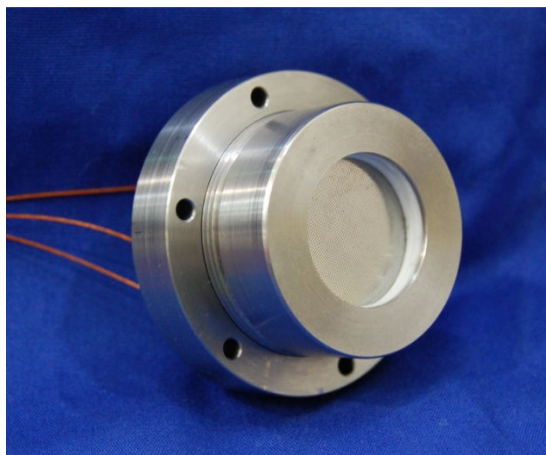

Figure 4. Four-grid retarding potential analyzer.

III. Experimental Results

    Figure 5 shows the thrust contour of the device as a function of power and magnetic field at three different mass flow rates. At 150 G and mass flow rates 3.0 mg/s and 4.5 mg/s, RF powers greater than 675 and 590 W, respectively, the plasma did not have a stable match and could not be maintained long enough to measure. Thrust is

primarily increased by increasing RF power, with a smaller gain from increasing the magnetic field and the mass flow rate. The impact of the magnetic field is not monotonic, as there is a region of higher thrust for low magnetic field strength.
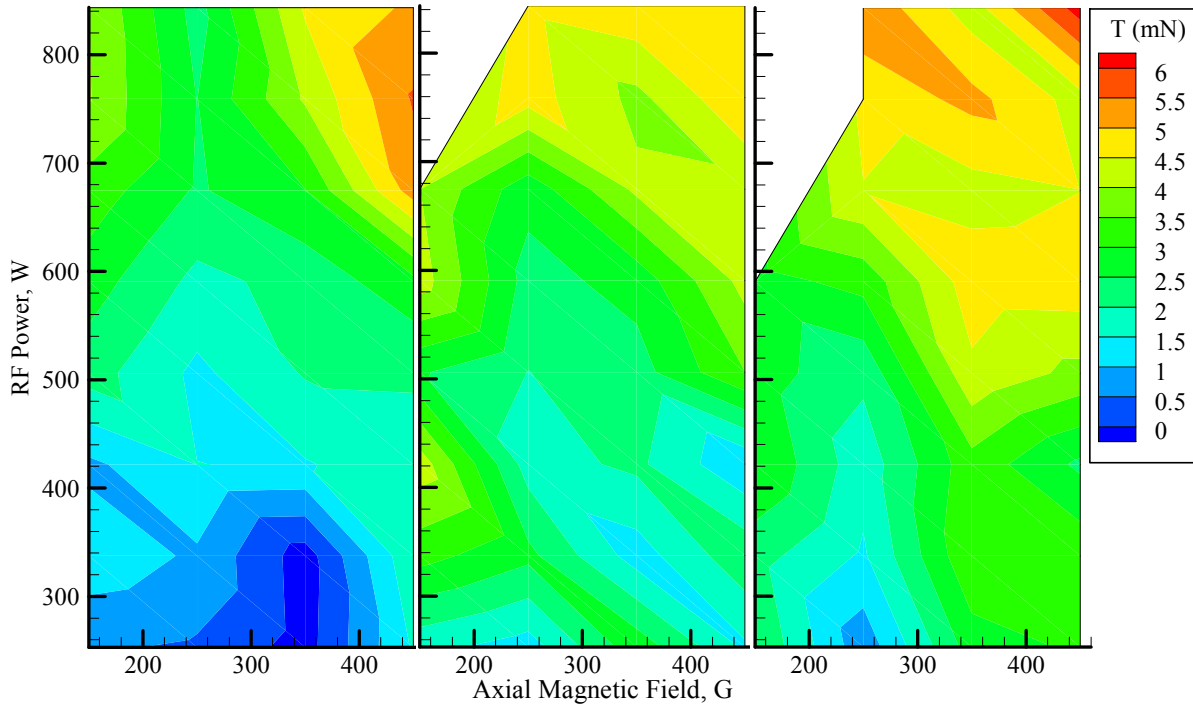

Figure 5. Helicon thrust contour as a function of power and magnetic field. 11.9 MHz, Ar (*left*) 1.5 mg/s, 2.0x10⁻⁵ Torr, (*center*) 3.0 mg/s, 2.3x10⁻⁵ Torr, (*right*) 4.5 mg/s, 2.6x10⁻⁵ Torr.

There are two other performance parameters of interest for any thruster: the efficiency, η_T, and specific impulse, I_{sp}, of the device. The total efficiency of the thruster is defined as,

$$\eta_T = \frac{T^2}{2\dot{m}P_{in}} \tag{2}$$

where T is the thrust, $\dot{m}$ is the mass flow rate, and P_{in} is the total input power. A more suitable method uses the anode efficiency, η_a, which only takes into account the power used to create and accelerate the ions, in this case just the RF power.

$$\eta_a = \frac{T^2}{2\dot{m}P_{RF}} \tag{3}$$

Figure 7 shows the efficiency of the device at 4.5 mg/s as a function of power and magnetic field. Efficiency is characteristically very low and somewhat independent of all three operating parameters, except at high power and high magnetic field strength where a low propellant flow rate increases efficiency by a factor of 3-4.
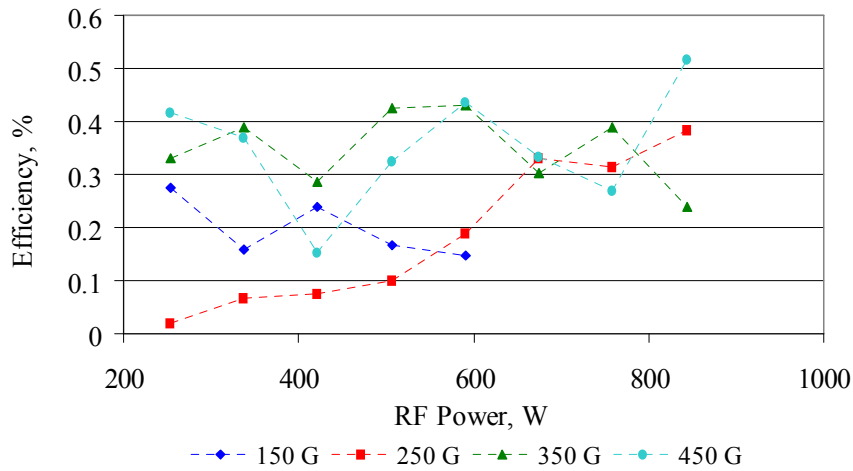
Figure 6. Anode efficiency as a function of power and magnetic field. 4.5 mg/s Ar, 11.9 MHz, 2.6x10^{-5} Torr.
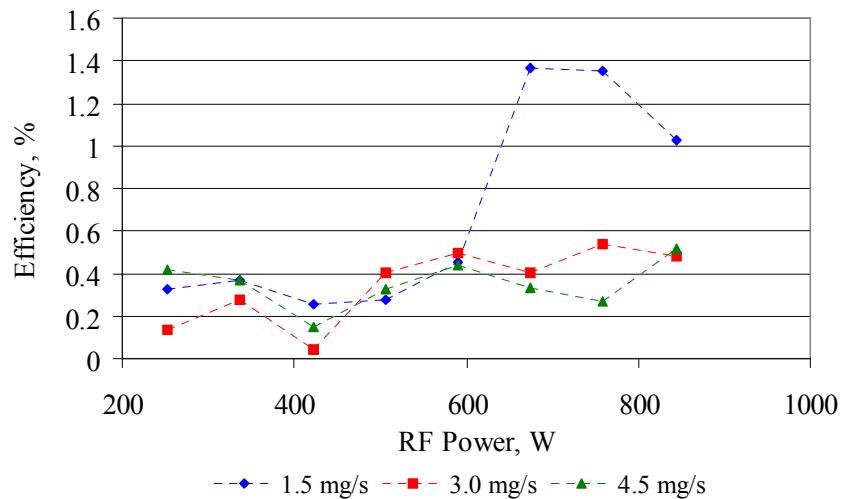

Figure 7. Anode efficiency as a function of power and mass flow. 450 G, Ar, 11.9 MHz, 2.0-2.6x10^{-5} Torr.

The other performance parameter of interest is the specific impulse, defined as

$$I_{sp} = \frac{T}{\dot{m}g} \tag{4}$$

where g is the acceleration due to gravity. The specific impulse of the device is shown below in Figure 8 and Figure 9. As before, for fixed mass flow rates the specific impulse increases slightly magnetic field strength except for low field strength where the specific increases as the magnetic field decreases. Unlike before, an increase in mass flow rate decreases specific impulse.
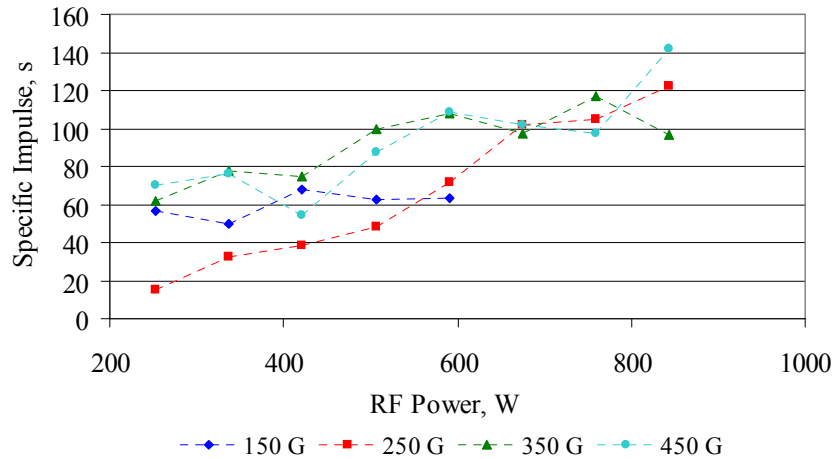
American Institute of Aeronautics and Astronautics

Figure 8. Specific impulse as a function of power and magnetic field. 4.5 mg/s Ar, 11.9 MHz, 2.6×10^{-5} Torr.
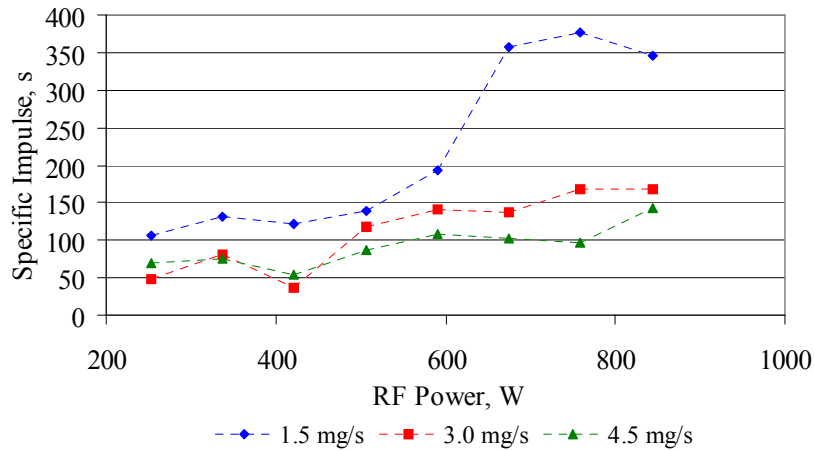

Figure 9. Specific impulse as a function of power and mass flow rate. 450 G, 11.9 MHz. Pressure is 2.0, 2.3, and 2.6×10^{-5} Torr for 1.5, 3.0, and 4.5 mg/s flow rates, respectively.

    The resulting ion energy distribution from the RPA is shown in Figure 10, with each distribution normalized by the maximum current collected by the RPA. The first observation seen from Figure 10 is that there are two primary peaks, with additional smaller peaks at high power. The voltage drop between the two populations is about 30 V, similar to the energy distributions measured by Takahashi,[19] giving the most probable exit velocity of about 12,000 m/s. The second observation is that increasing the power slightly increases the voltage at which the peaks occur. Finally, at 150 G increasing the power increases the population of the high energy ions, while at 350 G increasing the power has the opposite effect.
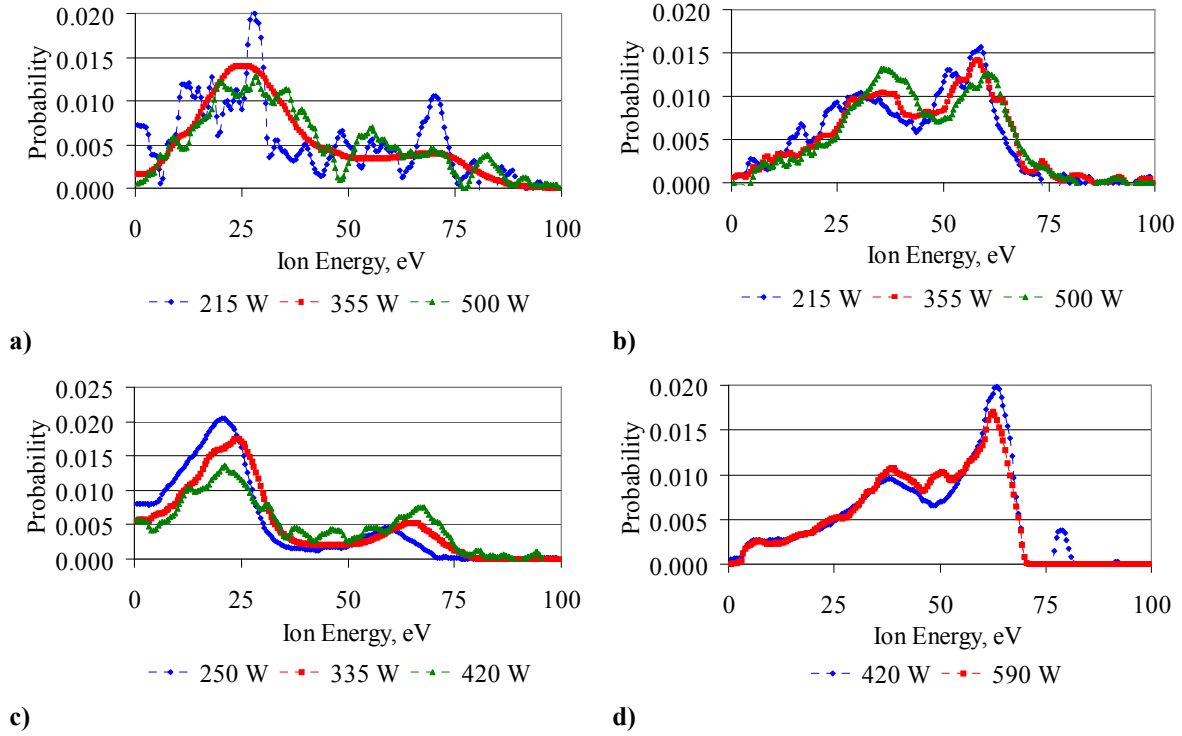
American Institute of Aeronautics and Astronautics

Figure 10. Ion energy distributions 45 cm downstream of the exit plane. 1.5 mg/s Ar, 2.0x10^{-5} Torr. a) 150 G, 13.56 MHz, b) 350 G, 13.56 MHz, c) 150 G, 11.9 MHz, d) 350 G, 11.9 MHz.

IV. Discussion

Thrust is not due simply to thermal ion exhaust. Assuming an ion temperature of 0.3 eV, which is a conservative upper bound estimation based on other works,[28-30] the axial ion exit velocity is only 850 m/s. At that exit velocity, the upper bound on thrust at full mass flow and maximum power would be 3.8 mN, which the data consistently exceeds at those conditions. Furthermore, it is not capable of providing the high ion velocities seen in excess of 10,000 m/s. A thermal mechanism would also explain neither the second energy peak nor the high energy tail of the distribution. Rather, the ion energy distributions clearly show multiple overlapping Gaussian populations, which suggest an ion population at the plasma potential and an ion beam under direct acceleration. This is supported by the fact that that the voltage of the low energy peak moves with RF power, as the plasma potential increases with increasing power.[31]

Along this line of inquiry, the ion energy distributions can be compared to the thrust data using specific impulse. Expanding on Eq. (4), thrust is defined as

$$T = \gamma \dot{m}_i v_i \tag{5}$$

where γ is the beam divergence factor, $\dot{m}_i$ is the ion mass flow rate, and v_i is the ion exit velocity. Equation (5) assumes that the ion exit velocity is much larger than the neutral exit velocity. Equation (5) can be substituted into Eq. (4), yielding an equation for the specific impulse in terms of ion exit velocity and mass utilization efficiency, η_m.

$$I_{sp} = \gamma \eta_m \frac{v_i}{g} \tag{6}$$

Thus, the values of the specific impulse calculated from the thrust measurements can be compared to the ion energy distributions using an average ion exit velocity. For this it is assumed that the low energy population corresponds to ions at the plasma potential and higher energy ion populations due to acceleration.[15] Therefore the center of the first peak corresponds to the plasma potential, and only ions past that energy are accelerated. From the data in Figure 10, the average ion exit velocity can be calculated using the equation

$$\bar{v}_i = \sum_j x_j \left(\frac{2e(V_j - V_p)}{m_i} \right)^{\frac{1}{2}}$$

(7)

where x_j is the probability at each voltage, V_j is the voltage of the jth term of the series, V_p is the plasma potential, and m_i is the mass of the ion. Figure 11 shows the estimated average ion exit velocity. At 150 G this average velocity increases with power, while at 350 G the trend is reversed. Furthermore, for the 13.56 MHz case the average velocity for 350 G is lower than at 150 G, and the same is true for the 11.9 MHz case where overlapping data is available.
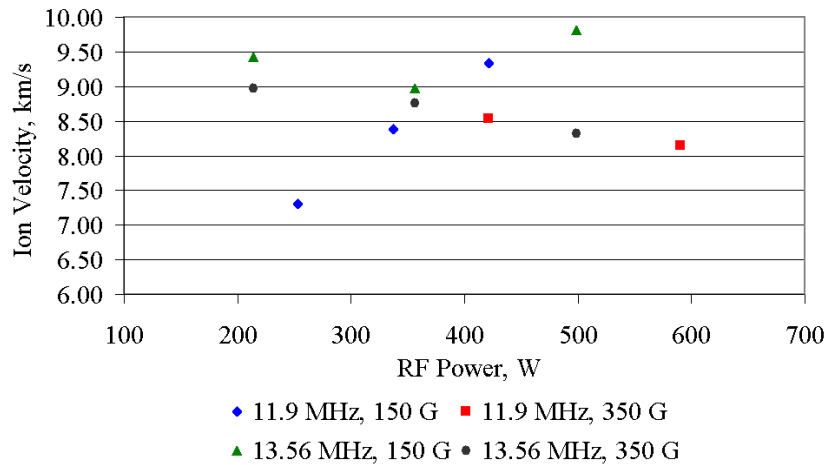

Figure 11. Average ion exit velocity as a function of power, frequency, and magnetic field. 1.5 mg/s Ar, 2.0×10^{-5} Torr.

The attenuated beam current density on the centerline of the device is measured by the RPA when the ion repulsion grid has no applied potential. Figure 12 shows that for either frequency or magnetic field strength, increasing the RF power increased the number of ions collected at the RPA. At 13.56 MHz the ion current increases by a factor between 2.1-2.7, while at 11.9 MHz the effect is more pronounced with an increase by a factor of 4.1. Increasing the magnetic field strength has been shown to increase the plasma density by a factor of 2 over that increase in magnetic field.[32] This increase in plasma density implicitly means an increase in ionization and thereby mass utilization. For the 11.9 MHz case it is possible that the increase is even larger due to a plasma coupling mode transition which results in a larger increase in ionization.[33-35]
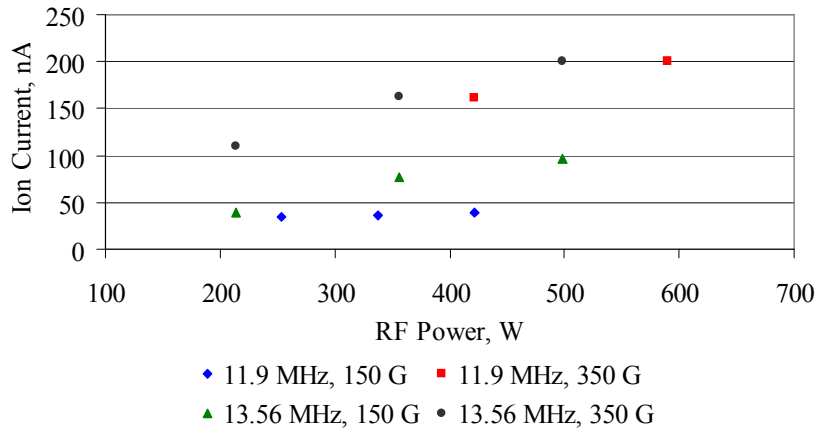
Figure 12. Maximum RPA collection current as a function of power, frequency, and magnetic field. 1.5 mg/s Ar, 2.0×10^{-5} Torr, 45 cm downstream of exit plane.

Figure 11 and Figure 12 explain part of the reason why the magnetic field has a smaller effect on the thrust than RF power. Increasing the magnetic field increases the density of the plasma and the beam current, yet at the same time decreases the average ion exit velocity. Therefore part of the thrust gain caused by the increase in beam current is mitigated by the decrease in average ion energy. For this same reason thrust is strongly dependant on RF power, since increasing power increases the number of ions. At 150 G it also increases the average ion velocity, while for 350 G it slightly decreases. However, the proportional loss of exit velocity is much less than the increase in ion current, e.g. only 3-15% and 200%, respectively, for increasing the magnetic field from 150 to 350 G. Thus the thrust increases overall with power since the increase in ion current dominates. For the case of low magnetic field strength and high power the reason thrust increases with a decreasing magnetic field is most likely due to a transition to a Trivelpiece-Gould plasma resulting in a higher ion density. Since the increase in thrust due to the magnetic field is much less pronounced there is another factor to consider – beam divergence.

The values in Figure 11 correspond to specific impulses between 700-1,000 s assuming no beam divergence and full mass utilization. Using Eq. (6) to compare the estimated average ion exit velocity to the calculated specific impulse, the product of the beam divergence factor and the mass utilization efficiency would have to equal between 0.05 and 0.22. The mass utilization efficiency increases with magnetic field, as more ions are created for the same mass flow rate, yet the increase in thrust is much smaller than the increase in beam current would suggest. Therefore the beam divergence factor must decrease with the magnetic field. This is most likely due to the higher magnetic field magnetizing more of the ions. The ion gyroradius is

$$ r_g = \frac{m_i v_\perp}{eB} \tag{8} $$

where $v_\perp$ is the perpendicular velocity of the ion with respect to the magnetic field, which is proportional to the square root of the ion temperature. Previous work has observed that the ion temperature increases with a one-to-one correlation or less with the magnetic field.[28,29] Thus, the perpendicular velocity increases more slowly with the magnetic field strength than the magnetic field itself, thus decreasing the gyroradius with the magnetic field. A change in magnetic field from 150 G to 350 G is estimated to change the gyroradius from 2.7 cm to 1.4 cm. This shows that increasing the magnetic field increases containment of the ions onto the field lines. As the magnetic field weakens past the exit plane more ions detach from the field lines, but at this point the ions already have a velocity divergent from the axis of the device. Figure 13 and Figure 14 show that increasing the magnetic field strength results in the magnetic contour lines extending further away from the discharge chamber. As an example, increasing the magnetic field from 150 G to 350 G extends the 150 G contour line out by 10 cm. This extension results in the ions being trapped on the magnetic field lines longer and becoming increasingly divergent and reducing thrust.
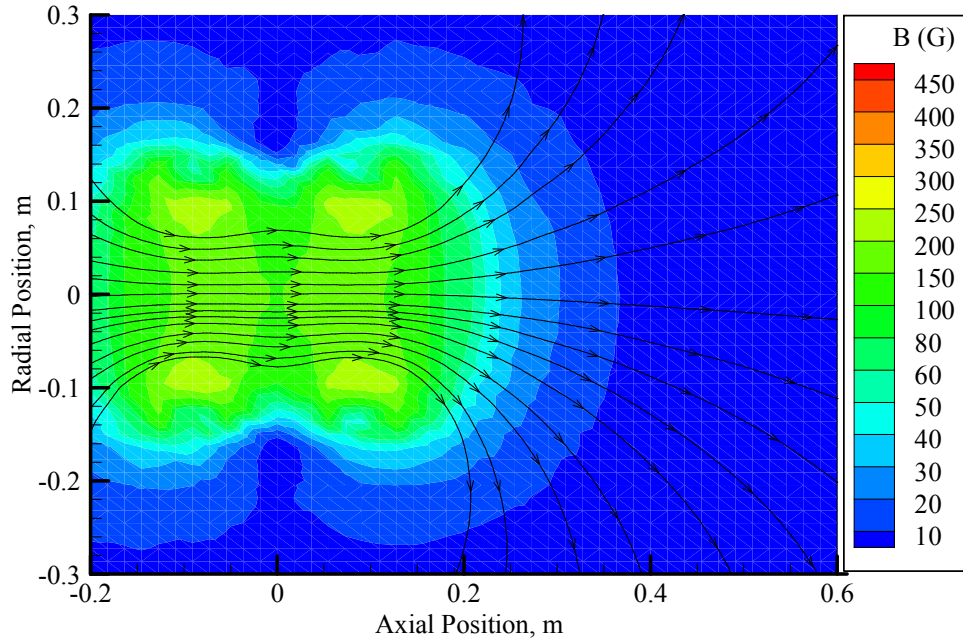
Figure 13. Magnetic field line and contour simulation. 3.76 coil current, 150 G nominal field.
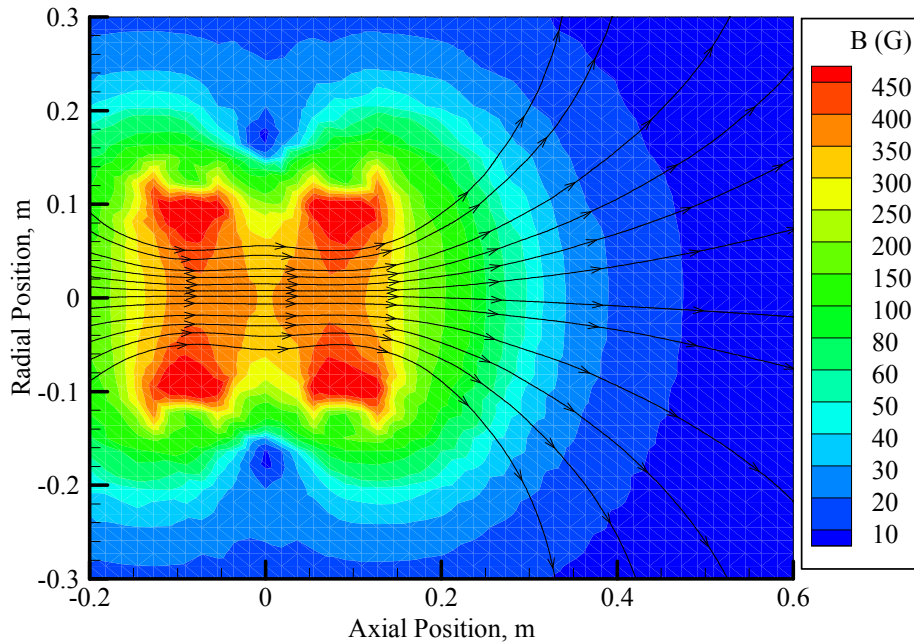

Figure 14. Magnetic field line and contour simulation. 8.76 coil current, 350 G nominal field.

The reason the RPA observes the increase in ion emission despite the increased field divergence is due to the center-line magnetic field lines experiencing the least amount of divergence, allowing the ions to detach from the weaker magnetic field prior to diverging from the axis. In Figure 13 and Figure 14 the RPA would appear at the edge of the plot at z = 0.6 and r = 0. Therefore, much of the gained thrust due to higher ion current is lost due to higher beam divergence, resulting in thrust gains that are within the bounds of the thrust stand noise and difficult to clearly observe. However, eliminating plume divergence would not completely solve the low performance of the device. Using the average ion velocities in Figure 11 and assuming no beam divergence and full mass utilization, the thrust is only between 10-14 mN which yields efficiencies between 6-20%, depending on the assumed ionization efficiency. This means that apart from any loss mechanism, most of the power goes into ion formation, not

acceleration. Therefore to improve performance beyond the gains from increased beam collimation or mass utilization, either additional power must be used to heat the ions to higher energies, or a second stage needs to be added to directly accelerate the ions.

The mass flow likewise has a smaller effect on thrust than RF power over the range of 1.5-4.5 mg/s. At the RF power range used ionization within the plasma is still power limited, evidenced by the large increases in ion current with power. Thus adding additional mass flow does not lead to a large increase in ionization. Increasing the mass flow rate does increase pressure within the discharge chamber as well as additional bulk flow energy, but these effects do not increase flow energy or ionization rate as much as increasing RF power. For the same reason increasing the mass flow greatly decreases specific impulse, since a negligible increase in thrust is paired with a large increase in mass flow, causing a decrease in thrust per weight of propellant.

While both the magnetic field and the mass flow rate alone do not affect thrust as effectively as RF power, combined they still have a noticeable impact. As an example, the two previous experiments observed less thrust than what is measured here. The thrust observed in Takahashi's experiment[19] is between 0-3 mN, with very similar ion energy distributions, with two primary peaks that increase in voltage with increasing RF power. The potential difference between the two peaks is also consistent. The power range is similar, 140-725 for Takahashi versus 215-840 here. The only discrepancies were the amount the magnetic field strength, 200 G versus 150-450 G and the mass flow rate, 0.6 mg/s versus 1.5-4.5 mg/s of argon, for Takahashi and the authors, respectively. The device in this work however demonstrated higher thrust by a factor of 2 over these operating conditions. One might consider the difference in performance is the size of the discharge chamber. One model[36] gives the thrust of a helicon as

$$T = n_e k T_e A \tag{9}$$

where A is the area of the exit plane of the discharge chamber. Therefore it is possible that the larger thrust seen here is due to a larger exit diameter, 14 cm versus 6.4 cm. However, a similar experiment by Pottinger[20] that used a helicon of the same diameter used here also saw thrust between 1-2.8 mN using 1.0 mg/s of krypton for RF powers of 250-650 W at a magnetic field strength of 100 G. Examining Figure 5, at 700 W increasing the magnetic field and mass flow rate together to the maximum values can increase the thrust by 50%. While it is a smaller increase than a similar increase in RF power would provide, it explains the difference in thrust between this experiment and the two previous studies.

V. Conclusion

The thrust of a helicon plasma source is measured across a range of mass flow rates, magnetic field strengths, RF powers, and RF frequencies. Maximum thrust is found to be 6.27 mN at a specific impulse of 142 s, and maximum specific impulse at 377 s at 5.55 mN. Thrust is not due to thermal ion exhaust, as estimated thermal thrust is less than the measured thrust. RPA scans of the plume also show a two peak structure that implies ion acceleration. Thrust primarily increases with RF power, with the magnetic field and mass flow rate increasing thrust by a smaller amount. Thrust increases are also achieved at high power and low magnetic field strength, potentially due to a transition to a Trivelpiece-Gould plasma. Over the operating ranges tested thrust is driven by ion creation more than changes in ion energy distributions. Collimation of the plume and increases in mass utilization efficiency would improve thrust performance, but efficiency would only reach a maximum of 30%. This indicates that increased ion heating or an acceleration stage is required to improve performance to reach parity with other electric propulsion devices.

Acknowledgments

References

[1]Chen, F. F., "Plasma Ionization by Helicon Waves," *Plasma Physics and Controlled Fusion*, Vol. 33, No. 4, 1991, pp. 339-364.
   [2]Boswel, R. W., "Very Efficient Plasma Generation by Whistler Waves Near the Lower Hybrid Frequency," *Plasma Physics and Controlled Fusion*, Vol. 26, No. 10, 1984, pp. 1147-1162.

[3]Chen, F. F. and Boswell, R. W., "Helicons – the Past Decade," *IEEE Transactions on Plasma Science*, Vol. 25, No. 6, 1997, pp. 1245-1257.

[4]Chen, F. F., "Experiments on Helicon Plasma Sources," *Journal of Vacuum Science and Technology*, Vol. 10, No. 4, 1992, pp. 1389-1401.

[5]Borg, G. G. and Boswell, R. W., "Power Coupling to Helicon and Trivelpiece-Gould Modes in Helicon Sources," *Physics of Plasmas*, Vol. 5, No. 3, 1998, pp. 564-571.

[6]Shamrai, K. P. and Taranov, V. B., "Volume and Surface RF Power Absorption in a Helicon Plasma Source," *Plasma Sources Science and Technology*, Vol. 5, No. 3, 1996, pp. 474-491.

[7]Kimura, S. and Ikoma, H., "Fowler-Nordheim Current Injection and Write/Erase Characteristics of Metal-Oxide-Nitride-Oxide-Si Structure Grown with Helicon-Wave Excited Plasma Processing," *Journal of Applied Physics*, Vol. 85, No. 1, 1999.

[8]Winglee, R. *et al*, "Simulation and Laboratory Validation of Magnetic Nozzle Effects for the High Power Helicon Thruster," *Physics of Plasmas*, Vol. 14, No. 6, 2007.

[9]Hwang, Y. S., Hong, I. S., and Eom, G. S., "Conceptual Design of a Helicon Ion Source for High-Current DC Accelerators," *Review of Scientific Instruments*, Vol. 69, No. 3, 1998, pp. 1344-1348.

[10]Hong, I. S. *et al*, "Ion-Beam Characteristics of Novel Helicon Ion Sources for Different Plasma Parameters," *Review of Scientific Instruments*, Vol. 71, No. 3, 2000, pp 1385-1388.

[11]Mordyk, S. *et al*, "Investigation of Helicon Ion Source Extraction Systems," *Review of Scientific Instruments*, Vol. 79, No. 2, 2008.

[12]Ziemba, T., *et al*, "High Power Helicon Thruster," *41st Joint Propulsion Conference and Exhibit*, July 2005, Tucson Arizona, AIAA 2005-4119.

[13]Charles, C., *et al*, "Helicon Double Layer Thrusters," 29th *International Electric Propulsion Conference*, Princeton New Jersey, 2005, IEPC-2005-290.

[14]Charles, C., Boswell, R. W., and Lieberman, M. A., "Xenon Ion Beam Characterization in a Helicon Double Layer Thruster," *Applied Physics Letters*, Vol 89, No. 26, 2006.

[15]West, M. D., Charles, C., and Boswell, R. W., "Testing a Helicon Double Layer Thruster Immersed in a Space-Simulation Chamber," *Journal of Propulsion and Power*, Vol. 24, No. 1, 2008, pp. 134-141.

[16]Charles, C. and Boswell, R. W., "Current-Free Double-Layer Formation in a High-Density Helicon Discharge," *Applied Physics Letters*, Vol. 82, No. 9, 2003, pp. 1356-1358.

[17]Cox, W. *et al*, "Spatial Retarding Field Energy Analyzer Measurements Downstream of a Helicon Double Layer Plasma," *Applied Physics Letters*, Vol. 93, No. 7, 2008.

[18]Ling, J. *et al*, "Thruster Measurements in a Low-Magnetic Field High-Density Mode in the Helicon Double Layer Thruster," *Journal of Physics D: Applied Physics*, Vol. 43, No. 30, 2010.

[19]Takahashi, K. *et al*, "Direct Thrust Measurement of a Permanent Magnet Helicon Double Layer Thruster," *Applied Physics Letters*, Vol. 98, No. 14, 2011.

[20]Pottinger, S. *et al*, "Performance Characterization of a Helicon Double Layer Thruster Using Direct Thrust Measurements," *Journal of Applied Physics D,* Vol. 44, No. 23, 2011.

[21]*Vacuum Measurement*, Varian, Inc., 2005, Available from: http://www.varianinc.com/cgi-bin/nav?products/vacuum/measure/index&cid=IPMHIKJQFO.

[22]MKS Product Specifications, *MKS 1179A Instruction Manual*, MKS Instruments, 2000, pp. 57.

[23]Xu, K. G. and Walker, M. L. R., "High-Power, Null-Type, Inverted Pendulum Thrust Stand," *Review of Scientific Instruments*, Vol. 80, No. 5, 2009.

[24]Hofer, R. R., "Development and Characterization of High-Efficiency, High Specific Impulse Xenon Hall Thrusters," *Aerospace Engineering*, Ph.D. Dissertation, University of Michigan, Ann Arbor MI, 2004.

[25]King, L. B., "Transport-Property and Mass Spectral Measurements in the Plasma Exhaust Plume of a Hall-Effect Space Propulsion System," *Aerospace Engineering*, Ph.D. Dissertation, University of Michigan, Ann Arbor MI, 1998.

[26]Hutchinson, I. H., *Principles of Plasma Diagnostics*, Cambridge: Cambridge University Press, 1987.

[27]Keickhafer, A. W. and Walker, M. L. R., "RF Power System for Thrust Measurements of a Helicon Plasma Source," *Review of Scientific Instruments*, Vol. 81, No. 7, 2010.

[28]Balkey, M. M. *et al*, "Ion Heating and Density Production in Helicon Sources near the Lower Hybrid Frequency," *Plasma Sources Science and Technology*, Vol. 10, No. 2, 2001, pp. 284-294.

[29]Scime, E. E. *et al*, "Control of Ion Temperature Anisotropy in a Helicon Plasma," *Plasma Sources Science and Technology*, Vol. 7, No. 2, 1998, pp. 186-191.

[30]Kline, J. L. *et al*, "RF Absorption and Ion Heating in Helicon Sources," *Physical Review Letters*, Vol. 88, No. 19, 2002.

[31]Kaeppelin, V., Carrère, M. and Faure, J. B., "Different Operation Regimes in a Helicon Plasma Source," *Review of Scientific Instruments*, Vol. 72, No. 12, 2001, pp. 4377-4382.

[32]Rayner, J. P. and Cheetham, A. D., "Helicon Modes in a Cylindrical Plasma Source," *Plasma Sources Science and Technology*, Vol. 8, No. 1, 1999, pp. 79-87.

[33]Chi, K., Sheridan, T. E., and Boswell, R. W., "Resonant Cavity Modes of a Bounded Helicon Discharge," *Plasma Sources Science and Technology*, Vol. 8, No. 3, 2002, pp. 421-431.

[34]Ellingboe, A. R. and Boswell, R. W., "Capacitive, Inductive and Helicon-Wave Modes of Operation of a Helicon Plasma Source," *Physics of Plasmas*, Vol. 3, No. 7, 2001, pp. 2797-2804.

[35]Keiter, P. A., Scime, E. E. and Balkey, M. M., Frequency Dependent Effects in Helicon Plasmas," *Physics of Plasmas*, Vol. 4, No. 7, 1997, pp. 2741-2747.

[36]Fruchtman, A., "Neutral Depletion in a Collisionless Plasma," *IEEE Transactions on Plasma Science*, Vol. 36, No. 2, 2008, pp. 403-413.